

Lumped-element two-section impedance-matched SNAIL parametric amplifier

D. Moskaleva,^{1,2} N. Smirnov,¹ D. Moskalev,¹ A. Ivanov,¹ A. Matanin,¹
D. Baklykov,¹ M. Teleganov,¹ V. Polozov,¹ V. Echeistov,¹ E. Malevannaya,¹
I. Korobenko,¹ A. Kuguk,¹ G. Nikerov,¹ J. Agafonova,¹ and I. Rodionov^{1,2,a)}

¹*FMN Laboratory, Bauman Moscow State Technical University, Moscow, 105005, Russia*

²*Dukhov Automatics Research Institute, VNIIA, Moscow, 127030, Russia*

a) **Author to whom correspondence should be addressed:** irodionov@bmstu.ru

Broadband impedance-matched Josephson parametric amplifiers are key components for high-fidelity single-shot multi-qubit readout. Nowadays, several types of impedance matched parametric amplifiers have been proposed: the first is an impedance-matched parametric amplifier based on a Klopfenstein taper, and the second is an impedance-matched parametric amplifier based on auxiliary resonators. Here, we present the quantum-limited 3-wave-mixing lumped-element SNAIL parametric amplifier with two-units impedance matching transformer. A two-pole Chebyshev matching network with shunted resonators based on parallel-plate capacitors and superconducting planar coil. Operating in a flux-pumped mode, we experimentally demonstrate an average gain of 15 dB across a 600 MHz bandwidth, along with an average saturation power of -107 dBm and quantum-limited noise temperature.

Josephson parametric amplifiers have become key components in quantum information processing¹ as multi-qubit readout fidelity can limit overall quantum algorithms accuracy². The dynamic range of parametric amplifiers and their noise temperature mostly define the readout fidelity. State-of-the-art quantum-limited parametric amplifiers allow realizing nondestructive high-fidelity single-shot readout of superconducting qubit³⁻⁶ and multiplexed qubits readout⁷⁻⁹. In addition, broadband Josephson parametric amplifiers is a key element for single-photon power measurements of microwave¹⁰⁻¹² and optical¹³ signals, ultrahigh efficient multi-resonator quantum memory readout¹⁴, fast high-quality resonators characterization¹⁵, quantum metrology¹⁶, and dark matter research¹⁷. At present, traveling wave parametric amplifiers (TWPA) demonstrate the highest dynamic range, but their noise temperature is much higher the quantum limit, which limit the quantum efficiency¹⁸⁻¹⁹.

Impedance-matched Josephson parametric amplifiers (IMPA) are one of the most perspective quantum-limited cryogenic amplifiers. The idea of using impedance matching for parametric amplifiers was first demonstrated by J. Martinis group at 2014²⁰. By using a Klopfenstein taper they changed the impedance slowly from 50 Ω (room temperature electronic impedance) to load

impedance $Z_L = 15 \Omega$. Later, this approach was realized by several scientific groups²¹⁻²³. IMPA based on the Klopfenstein taper demonstrated a 15 dB gain across bandwidth from 300 to 700 MHz, along with an average saturation power of -110 dBm. In 2015 the IMPA based on auxiliary resonators²⁴ was first demonstrated. Auxiliary resonators were realized on a PCB plate as a two-section Butterworth prototype. Later, impedance-matched parametric amplifiers based on the auxiliary resonator was realized on-chip²⁵⁻²⁸. It is characterized by a gain of at least 15 dB, 200 – 600 MHz bandwidth and the saturation power about -100...-90 dBm. The best result for IMPA dynamic range was demonstrate in Ref. 29.

One of the key disadvantages of the proposed solutions is distributed auxiliary resonators realization. This significantly limits the range of characteristic impedances (from 15 Ω to 150 Ω), and increases devices footprint. Usually, IMPA nonlinear resonators have a characteristic impedance lower than 15 Ω (by reducing the impedance of the auxiliary resonator one can limit the reflections). Moreover, in case of Klopfenstein taper-based amplifiers, it is necessary to fabricate a complex transmission line consisting of hundreds of variable capacitors.

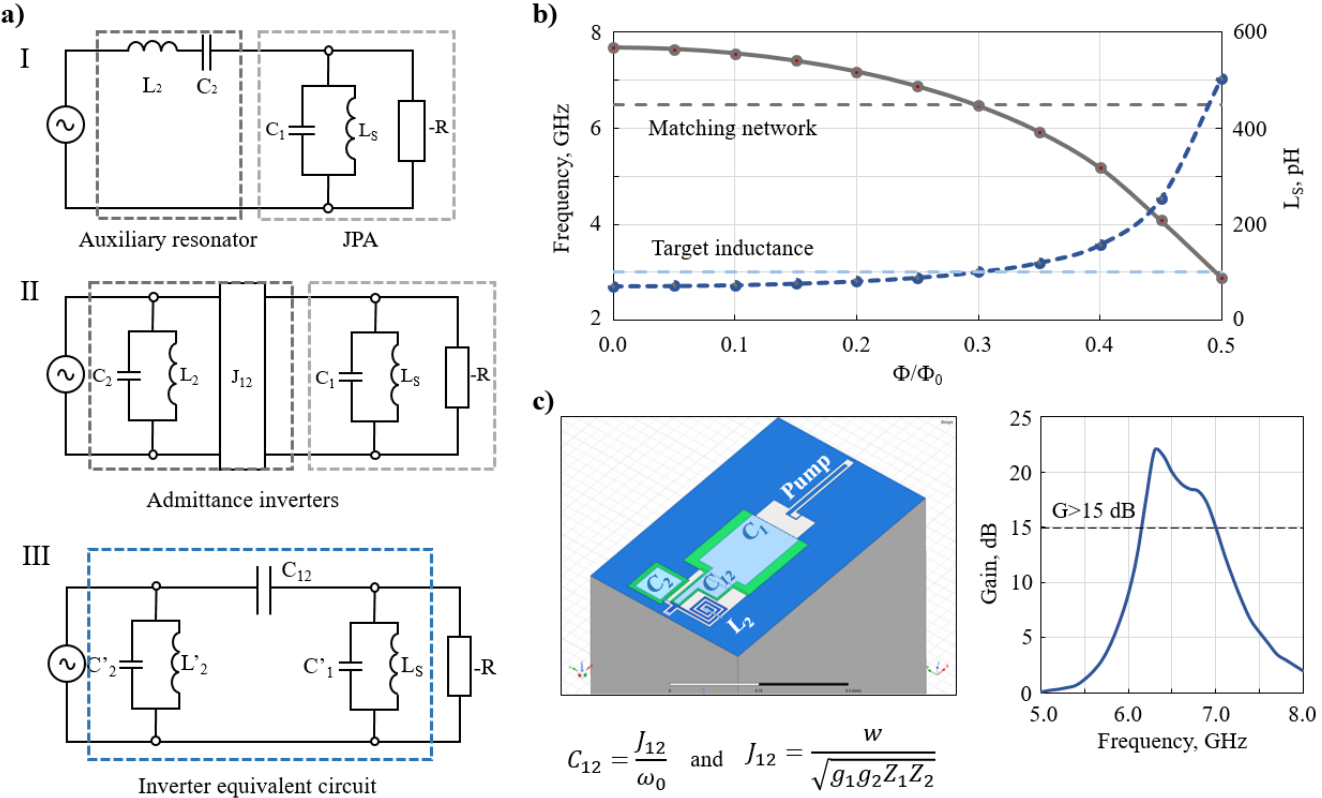


FIG. 1 Simulation results of IMPA with the two-pole Chebyshev matching network. (a) IMPA electric circuit transformation by the admittance inverters integrating. (b) Simulation of the IMPA tunable range for the asymmetry coefficient $a = 0.25$. (c) Simulation of IMPA resulting gain using Ansys HFSS

This problem can be solved by using lumped-element resonators²⁹⁻³⁰.

In this work, we present a broadband lumped-element impedance-matched parametric amplifier consisting of a single superconducting nonlinear asymmetric inductive element (SNAIL) and an on-chip two-pole Chebyshev matching network. Our amplifier operates in 3-wave-mixing reflection mode when the input signal reflects off, generating an amplified output signal with a gain of more than 15 dB and idler tone. We used a flux line to tune the SNAIL operating point. To improve the dynamic range of our parametric amplifier, we transform the environmental impedance, increasing coupling, lowering $Q = Z\omega C = Z/\omega L$ and using the single SNAIL proposed in previous works³¹⁻³³. We engineered the IMPA with an average gain of 15 dB across the 600 MHz bandwidth, along with an average saturation power of -107 dBm, and quantum-limited noise performance.

The impedance-matched parametric amplifier consists of a JPA and the on-chip two-pole impedance transformer. In our case, JPA is the LC oscillator realized

by the parallel connection of a single SNAIL with an inductance L_s and parallel plate capacitor with capacitance $C_1 = 5.25$ pF. The IMPA central resonance frequency is defined as $\omega_0 = 1/\sqrt{L_s C_1}$, where L_s define as follows:

$$L_s(\varphi_{ext}) = L_j/c_2(\varphi_{ext}), \quad (1)$$

where L_j – Josephson inductance of large junction in the loop, $c_2 = \alpha \cos \varphi_{min} + \frac{1}{3} \cos \left(\frac{\varphi_{min} - \varphi_{ext}}{3} \right)$ – flux-tunable constant, $\alpha = \frac{L_j(\text{large})}{L_j(\text{small})}$ – cell asymmetry, $\varphi_{ext} = 2\pi\Phi/\Phi_0$ – magnetic flux quantum and φ_{min} defined as $c_1 \equiv \alpha \sin \varphi_{min} + \sin \frac{\varphi_{min} - \varphi_{ext}}{3} = 0$. We choose SNAIL as a nonlinear element because its 3rd and 4th order (Kerr) nonlinearities depends on an external magnetic flux and possible to find the optimal operating point with negative Kerr nonlinearity while third-order nonlinearity depicted a 3-wave mixing process will be maximized. Limiting Kerr

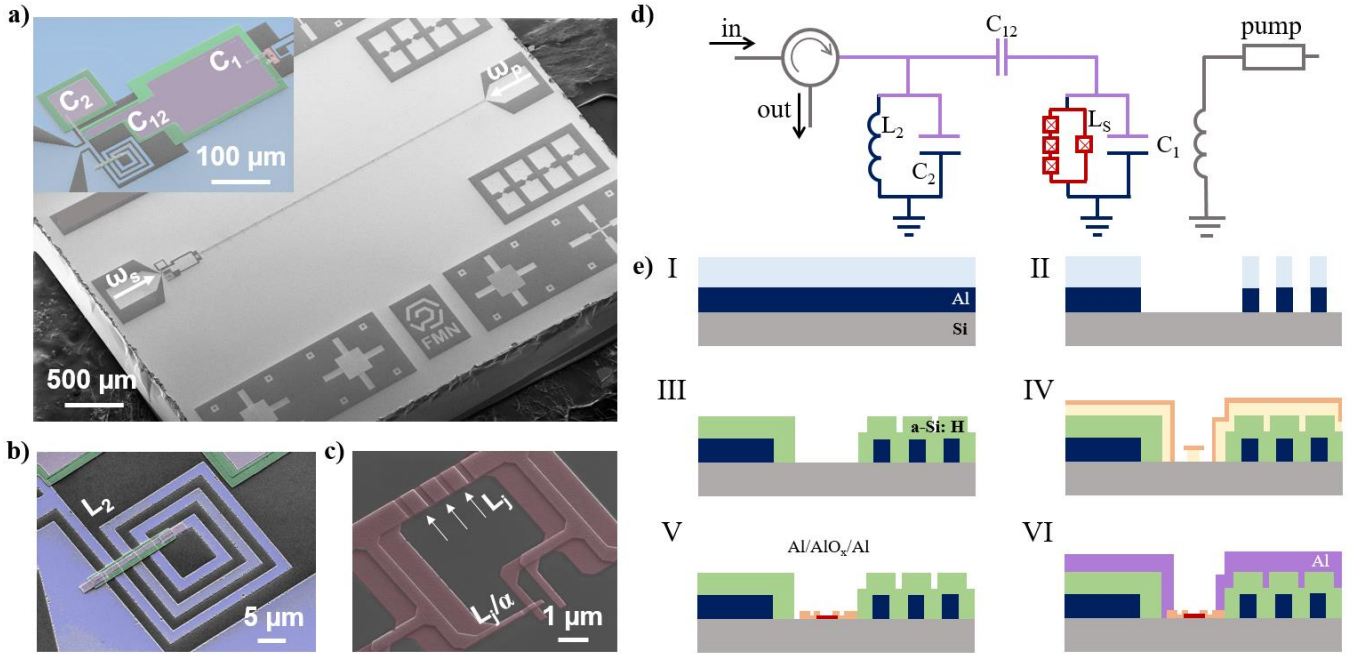


FIG. 2 IMPA with two-pole Chebyshev matching network. (a) Micrograph of the fabricated device with two limped-element resonators. (b) Higher-magnification micrograph of planar coil. (c) Higher-magnification micrograph of SNAL, which consists of an array of 3 large Josephson junctions in a loop with one smaller junction (red). (d) Circuit representation of the device. (e) IMPA fabrication steps.

nonlinearity improves the IMPA saturation power and maximizes the gain.

For the impedance transformer simulation, the negative-resistance prototype method proposed in Ref. 34 was utilized. We used the 2nd-order Chebyshev prototype (equal-ripple) to provide a multi-peak gain for the impedance transformer circuit. We chose prototype³⁴ with minimum gain $G_{\min} = 20$ dB, passband ripple 0.5 dB, and prototype coefficients are $g_1 = 0.5$, $g_2 = 0.24$ and $g_3 = 1.22$. The gain is defined as the ratio of the reflected power dissipated in the load resistance to the power available from the generator and can be described as follows:

$$G = |S_{11}|^2 = |\Gamma(\omega)|^2 = \frac{P_L(\omega) - 1}{P_L(\omega)}, \quad (2)$$

where $P_L(\omega) = 1 + k^2 T_N^2(\omega)$ – Chebyshev power loss function and $T_N = 2\omega^2 - 1$ – Chebyshev polynomial. On the other hand, the reflection coefficient $\Gamma(\omega)$ depends on the input impedance of IMPA circuit (Z_{in}): $\Gamma(\omega) = (Z_{in} - Z_0)/(Z_{in} + Z_0)$, where Z_{in} – the input impedance of IMPA. The bandwidth improvement of this IMPA is defined by fractional bandwidth w , which determine as $w = \frac{\omega_2 - \omega_1}{\omega_0}$, where $\omega_0 = \sqrt{\omega_1 \omega_2}$ – central resonance

frequency and R – negative resistance of parametric amplifier.

FIG. 1(a) shows the electrical circuit of the parametric amplifier formed by the negative-resistance prototype method. It consists of an alternating array of parallel and series resonators. However, resonators with characteristic impedance about $Z_{series} > 150 \Omega$ for series connection resonators and $Z_{shunt} < 15 \Omega$ for parallel connection cannot be realized by microstrip or coplanar transmission lines. That's why we used an admittance inverter for electrical circuit transformation³⁵ [see FIG. 1(b)]. In this study, the admittance inverter is a capacitance element that integrated into the electrical circuit, and it changes the resonator connection scheme. The inverter coupling capacitance depends on the inverter constant and the central resonance frequency of parametric amplifier ω_0 Eq. (3).

$$C_{ij} = \frac{J_{ij}}{\omega_0}, \quad (3)$$

where $J_{ij} = \frac{w}{\sqrt{g_i g_j Z_i Z_j}}$ – inverter constant, g_{ij} – Chebyshev prototype constants and Z_{ij} – impedance of the resonators.

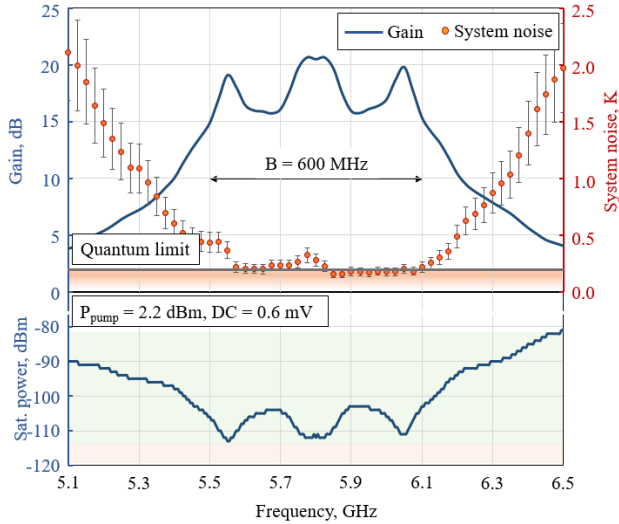


FIG. 3. Measured device performance operated at 10 mK. We demonstrate the amplifier performance at center frequency $\omega_a/2\pi = 5.8$ GHz. The IMPA provides an input saturation power of -107 dBm. The device shows a gain above 15 dB and operational bandwidth of nearly 600 MHz. We define the quantum limit as one photon $\hbar\omega$ of total system noise at the input of the amplifier.

We used the admittance inverter and resonators parallel connection because series resonator has a significant parasitic capacitance negatively influenced on the gain performance. Detailed calculation of the main IMPA parameters presented in [supplementary material](#).

We additional simulate the IMPA tunable range [see FIG. 1(e)]. The IMPA tunable range depends on an asymmetry coefficient (α) of single SNAIL. With increasing of the asymmetry coefficient, the tunable range of parametric amplifier is linearly increased. Maximum asymmetry is defined as $1/n$, where n – number of large Josephson junctions in the loop. In addition, we used Ansys HFSS to obtain the optimal gain profile.

FIG. 2 shows scanning electron microscopy images of the impedance-matched Josephson parametric amplifier and its fabrication process. Resonator 1 is formed by a capacitor $C_1 = 5.25$ pF that shunts the single SNAIL inductance L_S . SNAIL consists of an array of 3 large Josephson junctions (with Josephson inductance $L_J = 40$ pH) in a loop with one smaller junction (with inductance L_J/α) which has the asymmetry $\alpha = 0.25$ [see FIG. 2(c)]. We choose the asymmetry coefficient based on experimental dependence on the average parametric amplifier gain from α (see supplementary materials). The device was designed for the center frequency of $\omega_0/2\pi = 6.5$ GHz and fractional bandwidth of $\Delta\omega/2\pi = 500$ MHz.

Resonator 2 was implemented as lumped-element parallel LC resonator with $Z_2 = 12.7 \Omega$ [see FIG. 2(d)]. The coupling was realized by capacitors $C_{12} = 0.75$ pF. To prevent microwave-frequency slot modes, Al cross-overs were fabricated with the same dielectric as the capacitors placed on the pump port every 250 μm .

The IMPA fabrication process includes four main steps: (I, II) ground layer patterning (planar spiral coils, bottom capacitor electrodes, etc.), (III) dielectric layer deposition, (IV, V) SNAIL e-beam lithography, double-angle evaporation and lift-off, and (VI) evaporation of the top electrodes of the capacitors [see FIG. 2 (e)]. Before ground layer evaporation, silicon substrates were cleaned in Piranha solution at 80°C, and then 100-nm aluminum was deposited by electron-beam evaporation method. We used dry etching in Ar/Cl₂ for planar coils and bottom capacitor electrodes forming. A 350 nm thick hydrogen-saturated amorphous silicon (a-Si:H) layer was used as the dielectric layer in the capacitors. The PECVD method was used for dielectric stack deposition, and dry etch in CF₃/Ar was implemented for a-Si: H etch. Then, a bilayer mask was spin-coated onto the substrate, which consisted of 500 nm MMA (methyl methacrylate) and 150 nm AR-P (CSAR). The SNAIL is patterned using direct 50 kV e-beam lithography. Al/AlO_x/Al Josephson junctions are e-beam shadow-evaporated in a single vacuum cycle³⁶⁻³⁷. Lift-off was performed in a bath of N-methyl-2-pyrrolidone with sonication at 80°C for 3 hours and was rinsed in IPA with ultrasonication. The capacitor top electrodes were formed by a 600 nm thick Al.

Finally, we experimentally tested our amplifier in a dilution refrigerator with a base temperature below 10 mK. The cryogenic characterization has performed in a reflection mode with a circulator connected in series. The flux bias of the SNAIL loops was controlled by the flux line. Here, we define the operational bandwidth as the frequency range in which the gain is greater than 15 dB, and the noise temperature corresponds to the standard quantum limit. First, we determined the IMPA characteristic frequency by applying flux to SNAIL loop through a flux line. The resonant frequency in our case can be tuned from 4.9 to 8.2 GHz. Second, we chose the flux-bias operating point $\Phi_{DC} = 0.42\Phi_0$ and measure the gain response. We focused on areas with negative Kerr for SNAIL IMPA characterization.

FIG. 3 shows the best gain profile obtained at central frequency $\omega_{JPA} = 5.8$ GHz with a bandwidth of 600 MHz. This profile was obtained at the source pump power of $P_{pump} = 2.2$ dBm and flux line voltage of 0.6 mV. The

measuring device operates in 3-wave mixing mode. The saturation power of the amplifier is defined as a value of the input signal power at which the gain is decreased by 1 dB. The saturation power was measured at the same center frequency $\omega_{\text{JPA}} = 5.8$ GHz. We observed the saturation power of $-105\ldots-110$ dBm in the bandwidth of 600 MHz with a gain above 15 dB [see FIG. 3].

For the noise temperature measurements, we used the method described in Ref. [21]. We calibrated the noise of the HEMT following our IMPA, and then calculated the system noise using SNR improvement method. The estimated IMPA noise temperature is consistent with the near-quantum-limited operation [see FIG. 3].

In summary, we have designed, fabricated, and characterized the impedance-matched Josephson parametric amplifier based on the single SNAIL and the lumped-element impedance transformer based on the two-pole Chebyshev matching network. The proposed device has a stable gain profile, wide bandwidth, and the standard microelectronic fabrication process. We demonstrated an average gain of 15 dB across a 600 MHz bandwidth at the central resonance frequency of 5.8 GHz. The noise temperature was estimated to be close to the standard quantum limit with saturation power from -105 dBm to -110 dBm over the bandwidth. There is no need in $\lambda/4$ impedance transformer in the proposed design. The characteristic impedance of the auxiliary resonator ($12.7\ \Omega$) is quite difficult to realize by distributed transmission lines. Moreover, the lumped-element IMPA realization is feasible for further improvements by increasing of auxiliary resonators and easier integration of on-chip filters and circulators. Our amplifier is suitable for quantum information processing, such as multi-qubit readout, quantum vacuum measurements, and microwave photon detection.

The device was fabricated at the BMSTU Nanofabrication Facility (Functional Micro/Nanosystems, FMN REC, ID 74300).

AUTHOR DECLARATIONS

Conflict of Interest

The authors have no conflicts to disclose.

AUTHOR CONTRIBUTIONS

D. Moskaleva, N. Smirnov and D. Moskalev contributed equally to this work.

Daria Moskaleva: Conceptualization (equal); Formal analysis (lead); Methodology (equal); Investigation (lead);

Writing – original draft (lead). **Nikita Smirnov:** Conceptualization (equal); Formal analysis (lead); Investigation (lead); Writing – review and editing (equal). **Dmitry Moskalev:** Conceptualization (equal); Formal analysis (lead); Methodology (equal); Investigation (lead); Writing – review and editing (equal). **Anton Ivanov:** Formal analysis (equal); Investigation (equal); Writing – review and editing (equal). **Alexey Matanin:** Formal analysis (equal); Investigation (supporting); Writing – review and editing (supporting). **Dmitry Baklykov:** Investigation (supporting); **Maksim Teleganov:** Investigation (supporting); **Victor Polozov:** Investigation (supporting); **Vladimir Echeistov:** Investigation (supporting); **Elizaveta Malevannaya:** Investigation (supporting); **Igor Korobenko:** Investigation (supporting); **Alexey Kuguk:** Investigation (supporting); **Georgiy Nikerov:** Investigation (supporting); **Julia Agafonova:** Investigation (supporting); **Ilya Rodionov:** Project administration (lead); Conceptualization (lead); Formal analysis (equal); Writing – review and editing (equal).

DATA AVAILABILITY

The data that support the findings of this study are available within the article and its supplementary material.

REFERENCES

- ¹ D. M. Pozar, (John Wiley & Sons, Inc., 2010).
- ² Heinsoo J., Andersen C. K., Remm A., Krinner S., Walter T., Salathé Y., & Eichler C. “Rapid high-fidelity multiplexed readout of superconducting qubits,” *Phys. Rev. Appl.*, 10(3), 034040 (2018).
- ³ Lin, Z. R., Inomata, K., Oliver, W. D., Koshino, K., Nakamura, Y., Tsai, J. S., & Yamamoto, T. “Single-shot readout of a superconducting flux qubit with a flux-driven Josephson parametric amplifier,” *Appl. Phys. Lett.*, 103(13), 132602 (2013).
- ⁴ Abdo, B., Schackert, F., Hatridge, M., Rigetti, C., & Devoret, M. “Josephson amplifier for qubit readout,” *Appl. Phys. Lett.*, 99(16), 162506 (2011).
- ⁵ Smirnov, N.S., Krivko, E.A., Solovyova, A.A., Ivanov A.I. & Rodionov I.A. “Wiring surface loss of a superconducting transmon qubit,” *Sci Rep* 14, 7326 (2024).
- ⁶ Walter, T., Kurpiers, P., Gasparinetti, S., Magnard, P., Potočnik, A., Salathé, Y. & Wallraff, A. “Rapid high-fidelity single-shot dispersive readout of superconducting qubits,” *Phys. Rev. Appl.*, 7(5), 054020 (2017).
- ⁷ Macklin, C., O’Brien, K., Hover, D., Schwartz, M. E., Bolkhovsky, V., Zhang, X. & Siddiqi, I. “A near-quantum-limited Josephson traveling-wave parametric amplifier,” *Science*, 350(6258), 307-310 (2015).
- ⁸ White, T. C., Mutus, J. Y., Hoi, I. C., Barends, R., Campbell, B., Chen, Y. & Martinis, J. M. “Traveling

wave parametric amplifier with Josephson junctions using minimal resonator phase matching," *Appl. Phys. Lett.*, 106(24), 242601 (2015).

⁹ Kundu, S., Gheeraert, N., Hazra, S., Roy, T., Salunkhe, K. V., Patankar, M. P., & Vijay, R. "Multiplexed readout of four qubits in 3D circuit QED architecture using a broadband Josephson parametric amplifier," *Appl. Phys. Lett.*, 114(17), 172601 (2019).

¹⁰ Asztalos, S. J., Carosi, G., Hagmann, C., Kinion, D., Van Bibber, K., Hotz, M., & Clarke, J. "SQUID-based microwave cavity search for dark-matter axions," *Phys. Rev. Lett.* 104(4), 041301 (2010).

¹¹ Wallraff, A., Schuster, D. I., Blais, A., Frunzio, L., Majer, J., Devoret, M. H., & Schoelkopf, R. J. "Approaching unit visibility for control of a superconducting qubit with dispersive readout," *Phys. Rev. Lett.*, 95(6), 060501 (2005).

¹² Fedorov, G. P., Remizov, S. V., Shapiro, D. S., Pogosov, W. V., Egorova, E., Tsitsilin, I. & Ustinov, A. V. "Photon transport in a Bose-Hubbard chain of superconducting artificial atoms," *Phys. Rev. Lett.*, 126(18), 180503 (2021).

¹³ Kumar, P., Aytür, O., & Huang, J. "Squeezed-light generation with an incoherent pump," *Phys. Rev. Lett.*, 64(9), 1015–101 (1990).

¹⁴ Matanin, A. R., Gerasimov, K. I., Moiseev, E. S., Smirnov, N. S., Ivanov, A. I., Malevannaya, E. I. & Moiseev, S. A. "Towards highly efficient broadband superconducting quantum memory," *Phys. Rev. Appl.*, 19(3), 034011 (2023).

¹⁵ Zikiy, E.V., Ivanov, A.I., Smirnov, N.S. et al. "High-Q trenched aluminum coplanar resonators with an ultrasonic edge microcutting for superconducting quantum devices," *Sci Rep* 13, 15536 (2023).

¹⁶ Rosenthal, E. I., Schneider, C. M., Malnou, M., Zhao, Z., Leditzky, F., Chapman, B. J. & Lehnert, K. W. "Efficient and low-backaction quantum measurement using a chip-scale detector," *Phys. Rev. Lett.*, 126(9), 090503 (2021).

¹⁷ Kutlu, Ç., van Loo, A. F., Uchaikin, S. V., Matlashov, A. N., Lee, D., Oh, S. & Semertzidis, Y. K. "Characterization of a flux-driven Josephson parametric amplifier with near quantum-limited added noise for axion search experiments," *Superconductor Science and Technol.*, 34(8), 085013 (2021).

¹⁸ Perelshtain, M. R., Petrovnik, K. V., Vesterinen, V., Hamedani Raja, S., Lilja, I., Will, M. & Hakonen, P. J. "Broadband continuous-variable entanglement generation using a Kerr-free Josephson metamaterial," *Phys. Rev. Appl.*, 18(2), 024063 (2022).

¹⁹ Renger, M., Pogorzalek, S., Chen, Q., Nojiri, Y., Inomata, K., Nakamura, Y. & Fedorov, K. G. "Beyond the standard quantum limit for parametric amplification of broadband signals," *npj Quantum Inf.*, 7(1), 160 (2021).

²⁰ Mutus, J. Y., White, T. C., Barends, R., Chen, Y., Chen, Z., Chiaro, B. & Martinis, J. M. "Strong environmental coupling in a Josephson parametric amplifier," *Appl. Phys. Lett.*, 104(26), 263513 (2014).

²¹ Yang, R., & Deng, H. "Fabrication of the impedance-matched Josephson parametric amplifier and the study of the gain profile," *IEEE Trans. on Appl. Superconductivity*, 30(6), 1-6 (2020).

²² Huang K., Guo Q., Song C., Zheng Y., & Zheng D. "Fabrication and characterization of ultra-low noise narrow and wide band Josephson parametric amplifiers," *Chinese Phys. B*, 26 094203 (2017).

²³ Lu Y., Xu W., Zuo Q., Pan J., & Wu P. "Broadband Josephson parametric amplifier using lumped-element transmission line impedance matching architecture," *Appl. Phys. Lett.*, 120(8) 082601 (2022).

²⁴ Roy, T., Kundu, S., Chand, M., Vadiraj, A. M., Ranadive, A., Nehra, N. & Vijay, R. "Broadband parametric amplification with impedance engineering: Beyond the gain-bandwidth product," *Appl. Phys. Lett.*, 107(26), 262601 (2015).

²⁵ Grebel, J., Bienfait, A., Dumur, É., Chang, H. S., Chou, M. H., Conner, C. R. & Cleland, A. N. "Flux-pumped impedance-engineered broadband Josephson parametric amplifier," *Appl. Phys. Lett.*, 118(14), 142601 (2021).

²⁶ Duan, P., Jia, Z., Zhang, C., Du, L., Tao, H., Yang, X. & Guo, G. P. "Broadband flux-pumped Josephson parametric amplifier with an on-chip coplanar waveguide impedance transformer," *Appl. Phys. Exp.*, 14(4), 042011 (2021).

²⁷ Wu, S., Zhang, D., Wang, R., Liu, Y., Wang, S. P., Liu, Q. & Li, T. "Vacuum-gap-based lumped element Josephson parametric amplifier," *Chin. Phys. B*, 31(1), 010306 (2022).

²⁸ Ezenkova D., Moskalev D., Smirnov N., Ivanov A., & Rodionov I. "Broadband SNAIL parametric amplifier with microstrip impedance transformer," *Appl. Phys. Lett.*, 121(23) 232601 (2022).

²⁹ Kaufman R., White T., Dykman M., Iorrio A., Sterling G., Hong S., Opremcak A., Bengtsson A., Faoro L., Bardin J., Burger T., Gasca R., & Naaman O. "Josephson parametric amplifier with Chebyshev gain profile and high saturation," *Phys. Rev. Appl.*, 20(5), 054058 (2023).

³⁰ Ranzani, L., Ribeill, G., Hassick, B., & Fong, K. C. "Wideband Josephson parametric amplifier with integrated transmission line transformer," In 2022 IEEE Int. Conf. on Quant. Comp. and Eng. (QCE) (pp. 314-319) (2022).

³¹ Frattini, N. E., Vool, U., Shankar, S., Narla, A., Sliwa, K. M., & Devoret, M. H. "3-wave mixing Josephson dipole element," *Appl. Phys. Lett.*, 110(22), 222603 (2017).

³² Frattini, N. E., Sivak, V. V., Lingenfelter, A., Shankar, S., & Devoret, M. H. "Optimizing the nonlinearity and dissipation of a snail parametric amplifier for dynamic range," *Phys. Rev. Appl.*, 10(5), 054020 (2018).

³³ Sivak, V. V., Frattini, N. E., Joshi, V. R., Lingenfelter, A., Shankar, S., & Devoret, M. H. "Kerr-free three-wave

mixing in superconducting quantum circuits,” Phys. Rev. Appl., 11(5), 054060 (2019).

³⁴ Getsinger, W. “Prototypes for Use in Broadbanding Reflection Amplifiers,” J. IEEE Trans. on Microwave Theory and Techn. 11.6: 486-497 (1963).

³⁵ Naaman, O., and Aumentado. J. “Synthesis of Parametrically Coupled Networks,” PRX Quantum 3.2: 020201 (2022).

³⁶ Pishchimova A.A., Smirnov N.S., Ezenkova D.A., Krivko E.A., Zikiy E.V., Moskalev D.O., Ivanov A.I.,

Korshakov N.D., & Rodionov I.A. “Improving Josephson junction reproducibility for superconducting quantum circuits: junction area fluctuation,” Sci. Rep. 13, 6772 (2023).

³⁷ Moskalev D.O., Zikiy E.V., Pishchimova A.A., Ezenkova D.A., Smirnov N.S., Ivanov A.I., Korshakov N.D., & Rodionov I.A. “Optimization of shadow evaporation and oxidation for reproducible quantum Josephson junction circuits,” Sci. Rep. 13, 4174 (2023).